document 13321:1996) and histogram of size distribution. The ζ-potentials of micelles were measured by laser Doppler electrophoresis in 10 mM HEPES buffer (pH 7.4) containing 150 mM NaCl at 37 °C. All samples were equilibrated to the defined temperature for 2 h prior to measurement. Atomic force microscopy (AFM) imaging of the siRNA complexes was carried out in air using a Bruker AXS MMAFM Nanoscope V (Madison, WI) operated by Scan Assist with a standard silicon probe on the freshly cleaved mica substrate. Raw AFM images were processed by flattening to remove the background slope of the substrate surface.

***In Vitro* Micelle Stability.** Micelle stability was measured in the presence of 150 and 600 mM NaCl in the presence or absence of the disulfide reducing agent DTT. Micelle samples were diluted 1:1 with NaCl solution at desired concentrations and incubated at 37 °C for 24 h. Samples subjected to disulfide reducing conditions were diluted in the same fashion as above, however, with NaCl solutions containing 200 mM DTT. After the 24 h incubation period, samples were measured by static and dynamic light scattering as described in the micelle characterization section. Relative micelle stability was determined by dividing the scattered light intensity of treated samples with the scattered light intensity of samples diluted in the same fashion with only HEPES buffer.

***In Vitro* Gene Silencing.** HeLa human cervical cancer cells stably expressing luciferase (HeLa-luc) were seeded onto 35 mm Petri dishes (25 000 cells/dish) and allowed to attach for 24 h. After cell attachment, the medium was removed and replaced with media (2 mL) containing 100 μM luciferin and cross-linked micelles (200 nM siRNA). For each analysis, control samples were prepared by addition of media diluted with HEPES instead of micelle solution. The total dilution of media after addition of luciferin and micelle solution was less than 200 μL additives per 10 mL of media. Samples were placed into a Kronos real-time photon countable incubator, and the luminescence intensity was measured periodically over a 50 h time period, with the temperature and CO_2 maintained at 37 °C and 5%. Relative luminescence was determined by dividing the average luminescence intensity of treated samples by the average luminescence intensity of control samples, $n = 4$. Cells were cultured in Dulbecco's modified Eagle's medium (DMEM) containing 10% fetal bovine serum (FBS) and antiobiotics during the experiment.

Cytotoxicity. HeLa-luc cells were seeded onto 24-well plates (10 000 cells/well) and allowed to attach for 24 h under standard cell culture conditions. Next, the medium was removed and replaced with fresh media supplemented with cross-linked micelles at the desired siRNA concentration. Cells were further incubated with micelle-containing media for 48 h. Metabolism was assessed following 1 h incubation with cell counting kit 8 solution (1 μL/10 μL media) (CCK 8, Dojindo Laboratories, Kumamoto, Japan) followed by absorbance measurement of extracellular media at 450 nm. All data are expressed relative to untreated control cells, $n = 6$.

Cell Uptake. HeLa-luc cells were seeded onto 6-well plates (100 000 cells/well) and allowed to attach for 24 h. After the attachment period, medium was exchanged with fresh media containing micelles prepared with Cy3-siRNA (300 nM). Cells were incubated with micelle-containing media for 2 h under standard cell culture conditions then rinsed four times with PBS and harvested by trypsinization. Harvested cells were subjected to flow cytometric analysis using a BD LSR II instrument (BD Biosciences, San Jose, CA) equipped with appropriate excitation/emission filter combinations, and forward and side-scatter gates were set to exclude debris. A total of 10 000 events were recorded for each analysis, and data were analyzed using BD FACSDiva software (BD Biosciences).

***In Vitro* Confocal Microscopy.** HeLa-luc cells (50 000 cells) were seeded onto a 35 mm glass bottom dish (Iwaki, Tokyo, Japan) and allowed to attach for 24 h. Micelles were prepared with Cy5 siRNA (2IT-95) or Cy3 siRNA (cRGD-2IT-95) and introduced simultaneously to cells (500 nM siRNA each) followed by incubation for 4 h. After incubation with micelles, the medium was exchanged with fresh media containing LysoTracker Green (Invitrogen Molecular Probes, Eugene OR) and Hoechst 33342 (Dojindo Laboratories, Kumamoto, Japan), and the cells were incubated for an additional 15 min. Cells were rinsed with PBS containing Ca^{2+} and Mg^{2+} and imaged in this buffer. Confocal laser scanning microscopy was performed in live cells using a LSM 510 (Carl Zeiss, Oberlochen, Germany) with a C-Apochromat 63× objective (Carl Zeiss) and appropriate excitation sources and emission filters. Data were analyzed using LSM imaging software (Carl Zeiss). Colocalization was determined with respect to Cy3, Cy5, and LysoTracker using the following equation: relative colocalization = $\Sigma pixels_{colocalized}/\Sigma pixels_{total}$.

Blood Circulation. Micelle stability in the blood compartment was evaluated using intravital confocal laser scanning microscopy (IVRTCLSM) in live mice. All picture/movie acquisitions were performed using a Nikon A1R confocal laser scanning microscope system attached to an upright ECLIPSE FN1 (Nikon Corp., Tokyo, Japan) equipped with a 20× objective, 640 nm diode laser, and a band-pass emission filter of 700/75 nm. The pinhole diameter was set to result in a 10 μm optical slice. Eight-week-old female BALB/c nude mice (Oriental Yeast Co., Ltd., Tokyo, Japan) were anesthetized with 2.0−3.0% isoflurane (Abbott Japan Co., Ltd., Tokyo, Japan) using a Univenter 400 anaesthesia unit (Univentor Ltd., Zejtun, Malta). Mice were then subjected to lateral tail vein catheterization with a 30 gauge needle (Dentronics Co., Ltd., Tokyo, Japan) connected to a nontoxic, medical grade polyethylene tube (Natsume Seisakusho Co., Ltd., Tokyo, Japan). Anesthetized mice were placed onto a temperature-controlled pad (Thermoplate; Tokai Hit Co., Ltd., Shizuoka, Japan) integrated into the microscope stage and maintained in a sedated state throughout the measurement. Ear-lobe dermis was observed without surgery following fixation beneath a coverslip with a single drop of immersion oil. Data were acquired in video mode for 3 min (30 frames/s), followed by snap-shots every 1 min thereafter. All animal experimental procedures were performed in accordance with the Guide for the Care and Use of Laboratory Animals as stated by the National Institutes of Health.

Micelles prepared with Cy5-labeled siRNA were injected (200 μL of 9.2 μM siRNA, ~24 μg total siRNA) *via* the tail vein 10 s after the start of video capture. Video data were analyzed by selecting regions of interest (ROIs) within blood vessels or extravascular skin tissue, and the average fluorescence intensity per pixel for each time point was determined using the Nikon NIS-Elements C software provided by the manufacturer. To produce the blood retention profiles shown in Figure 6, vein fluorescence data were expressed relative to the maximum observed value (typically 45 s to 1 min.). First, the background fluorescence intensity was determined from video captured during the 10 s before sample injection. This background value was subtracted from the average pixel intensities measured after micelle injection to create background-corrected intensities for each time point. Next, relative fluorescence intensities were determined by dividing the average fluorescence intensity at each time point by the maximum observed fluorescence intensity. Each experiment was performed in triplicate in separate animals. A detailed description of the microscope apparatus and mouse positioning for IVRTCLSM, as well as examples of data workup showing ROIs, can be found in our previously published report.[35] Half-lives were calculated by plotting the natural log of intensity *versus* time for the initial period of signal decay (10 min for naked siRNA and 2IT-0, 15 min for 2IT-95). The slope of these plots were determined and applied to the half-life equation: $T_{1/2} = 0.693/(-\text{slope})$. Areas under the curve values were calculated using the trapezoid rule.

Biodistribution. HeLa-luc tumors were prepared by *in vivo* passage of solid tumor fragments. Donor tumors were prepared by injecting HeLa-luc cells (2.6×10^6 cells) under the skin in the right rear flank of BALB/c nude mice and allowed to mature for 2 weeks. After 2 weeks, donor tumors were excised and cut into 3 × 3 mm pieces. Tumor fragments were transplanted under the skin into the rear flank of 6 week old female BALB/c nude mice, and the wound was closed with a suture. Tumors were allowed to mature for 8 days, then mice were randomly assigned into treatment groups ($n = 4$ per group). Mice were fed alfalpha-free chow for 2 weeks before injecting micelle samples. Micelles prepared with Cy5.5 siRNA were injected (200 μL of 9.2 μM siRNA, ~24 μg total siRNA) *via* the tail vein.

After 24 h, mice were sacrificed and individual organs were excised and rinsed with PBS. Organs and tumors were imaged using an IVIS instrument in fluorescence mode with appropriate excitation and emission filters. Data were analyzed using Living Image software by drawing ROIs around whole organs to determine the total photon counts and signal area in square centimeters. The fluorescence intensity was normalized to sample area and irradiation time using the following equation: intensity = total photons/[illumination time (s) × area (cm^2)].

***In Vivo* Confocal Microscopy.** Micelles prepared with Cy5 siRNA were injected (200 μL of 9.2 μM siRNA, ~24 μg total siRNA) *via* the tail vein into mice bearing subcutaneous HeLa-H2BGFP tumors. HeLa-H2BGFP cells express green fluorescent protein (GFP) in the cell nucleus, which allows identification of tumor cells. After 24 h, mice were anesthetized and Hoechst 33342 dye (8 mg/kg in PBS, Lonza Group Ltd., Basel, Switzerland) was used to stain the nuclei of cells present in circulation and the perivascular space. Next, the tumor was exposed by a series of dorsal cuts in the skin surrounding the tumor to create a hinged skin flap with the tumor attached to the skin, while leaving blood vessels feeding the tumor intact. The exposed tumor was mounted under a coverslip and imaged using the IVRTCLSM equipped with a 40 or 60× objective. Hoechst, GFP, and Cy5 signals were detected simultaneously using 405, 488, and 640 nm excitation lasers and band-pass emission filters of 450/50, 525/50, and 700/75 nm, respectively. Images were analyzed using the Nikon NIS-Elements C software provided by the manufacturer.

Tumor Growth Inhibition. HeLa-luc tumors were prepared by *in vivo* passage of solid tumor fragments. Donor tumors were prepared by injecting HeLa-luc cells (2.6 × 10^6 cells) under the skin in the right rear flank of mice and allowed to mature for 2 weeks. After 2 weeks, donor tumors were excised and cut into 3 × 3 mm pieces. Tumor fragments were transplanted under the skin into the rear flank of 6 week old female BALB/c nude mice, and the wound was closed with a suture. Tumors were allowed to mature for 4 days, then mice were randomly assigned into treatment groups (n = 4 per group).

Micelle formulations were screened for *in vivo* efficacy using a combination therapy of VEGFR2 and VEGF siRNAs. Micelles were prepared to contain either type of siRNA in different micelle formulations and were injected separately. Micelle treatment began on day four following tumor implantation. Micelles containing VEGFR2 siRNA were injected on the first day of treatment, micelles incorporating VEGF siRNA were injected on day two, followed by two days with no injection. This sequence was repeated three times for a total of three injections of each micelle formulation and six total injections of micelles. For each injection, 200 μL of micelle solution (9.2 μM siRNA, ~24 μg total siRNA) was administered. The negative control sample for cRGD-2IT-95 formulation was prepared with scramble siRNA and was administered in the same fashion as described above. Tumor size was monitored over time by caliper measurement, and tumor volumes were calculated using the following equation: volume = $^1/_2 a \times b^2$, where a is the long axis and b is the short axis measured.

For determining the effect of each siRNA sequence individually (delivered by cRGD-2IT-95 micelles), subcutaneous tumors were prepared by *in vivo* passage as described above and the injection sequence used was the same, except for samples delivering only one type of siRNA. For groups receiving only one type of siRNA (VEGF or VEGFR2), micelles containing scramble siRNA were injected on the second day to keep the total amount of siRNA micelles injected into each mouse constant. Each group consisted of four mice, with additional data from other groups (HEPES, scramble, and VEGF+VEGFR2 treatment) combined in Figure 9.

PCR Analysis. Tumors were excised from mice 72 h after the last injection of micelles, and ~20 mg of non-necrotic tissue was selected from the tumor mass (n = 4 tumors, each tumor was analyzed in triplicate). Tumor fragments were sonicated for 10 s in lysis buffer and then centrifuged to remove excess debris. RNA was extracted from the supernatant using a RNeasy Mini Kit (Qiagen, Valencia, CA) according to the manufacturer's instructions. Extracted RNA samples were normalized to the same 260 nm absorbance value, and genomic DNA was eliminated, followed by RNA transcription to cDNA using a QuantiTect reverse transcription kit (Qiagen, Valencia, CA). RNA was quantified following conversion to cDNA and amplified using real-time PCR. Primers used for human actin and human VEGF were synthesized by Hokkaido System Science (Hokkaido, Japan), and the sequences used were as follows: CCAACCGCGAGAAGATGA (actin forward); CCAGAGGCGTACAGGGATAG (actin reverse); AGTGGTCCCAGGCTGCAC (VEGF forward); TCCATGAACTTCACCACTTCGT (VEGF reverse).

Statistical Analysis. All data are expressed as the average value ± the standard deviation. The p values were determined by the Student's t test using a two-tailed distribution and two-sample unequal variance with the T.Test function of Microsoft Excel. The p values of less than 0.05 were considered as statistically significant.

Conflict of Interest: The authors declare no competing financial interest.

Acknowledgment. This research was financially supported by the Funding Program for World-Leading Innovative R&D in Science and Technology (FIRST), and the Core Research Program for Evolutional Science and Technology (CREST) from the Japan Science and Technology Agency (JST). Additional support was provided to R.J.C. by the Japan Society for the Promotion of Science postdoctoral fellowship program. We thank T. Kanda (Aichi Cancer Center Research Institute) for HeLa H2B-GFP cells.

Supporting Information Available: Light scattering intensity of polymer and siRNA mixtures at different molar ratios, and stability of cRGD-2IT-95 and 2IT-95 micelles at 600 mM NaCl is provided. This material is available free of charge *via* the Internet at http://pubs.acs.org.

REFERENCES AND NOTES

1. Fire, A.; Xu, S.; Montgomery, M.; Kostas, S.; Driver, S.; Mello, C. Potent and Specific Genetic Interference by Double-Stranded RNA in *Caenorhabditis elegans*. *Nature* **1998**, *391*, 806–811.
2. Carthew, R.; Sontheimer, E. Origins and Mechanisms of miRNAs and siRNAs. *Cell* **2009**, *136*, 642–655.
3. Judge, A.; MacLachlan, I. Overcoming the Innate Immune Response to Small Interfering RNA. *Hum. Gene Ther.* **2008**, *19*, 111–124.
4. Robbins, M.; Judge, A.; MacLachlan, I. siRNA and Innate Immunity. *Oligonucleotides* **2009**, *19*, 89–101.
5. Turner, J.; Jones, S.; Moschos, S.; Lindsay, M.; Gait, M. MALDI-TOF Mass Spectral Analysis of siRNA Degradation in Serum Confirms an RNAse A-like Activity. *Mol. Biosyst.* **2007**, *3*, 43–50.
6. van de Water, F.; Boerman, O.; Wouterse, A.; Peters, J.; Russel, F.; Masereeuw, R. Intravenously Administered Short Interfering RNA Accumulates in the Kidney and Selectively Suppresses Gene Function in Renal Proximal Tubules. *Drug Metab. Dispos.* **2006**, *34*, 1393–1397.
7. Gary, D.; Puri, N.; Won, Y. Polymer-Based siRNA delivery: Perspectives on the Fundamental and Phenomenological Distinctions from Polymer-Based DNA Delivery. *J. Controlled Release* **2007**, *121*, 64–73.
8. Whitehead, K.; Langer, R.; Anderson, D. Knocking Down Barriers: Advances in siRNA Delivery. *Nat. Rev. Drug Discovery* **2009**, *8*, 129–138.
9. Xie, F.; Woodle, M.; Lu, P. Harnessing *In Vivo* siRNA Delivery for Drug Discovery and Therapeutic Development. *Drug Discovery Today* **2006**, *11*, 67–73.
10. Li, C.; Parker, A.; Menocal, E.; Xiang, S.; Borodyansky, L.; Fruehauf, J. Delivery of RNA Interference. *Cell Cycle* **2006**, *5*, 2103–2109.
11. Gao, K.; Huang, L. Nonviral Methods for siRNA Delivery. *Mol. Pharmaceutics* **2009**, *6*, 651–658.
12. Howard, K. Delivery of RNA Interference Therapeutics Using Polycation-Based Nanoparticles. *Adv. Drug Delivery Rev.* **2009**, *61*, 710–720.
13. Tan, S.; Kiatwuthinon, P.; Roh, Y.; Kahn, J.; Luo, D. Engineering Nanocarriers for siRNA Delivery. *Small* **2011**, *7*, 841–856.

14. Castanotto, D.; Rossi, J. The Promises and Pitfalls of RNA-Interference-Based Therapeutics. *Nature* **2009**, *457*, 426–433.
15. Matsumoto, S.; Christie, R. J.; Nishiyama, N.; Miyata, K.; Ishii, A.; Oba, M.; Koyama, H.; Yamasaki, Y.; Kataoka, K. Environment-Responsive Block Copolymer Micelles with a Disulfide Cross-Linked Core for Enhanced siRNA Delivery. *Biomacromolecules* **2009**, *10*, 119–127.
16. Christie, R.; Miyata, K.; Matsumoto, Y.; Nomoto, T.; Menasco, D.; Lai, T.; Pennisi, M.; Osada, K.; Fukushima, S.; Nishiyama, N.; Yamasaki, Y.; Kataoka, K. Effect of Polymer Structure on Micelles Formed between siRNA and Cationic Block Copolymer Comprising Thiols and Amidines. *Biomacromolecules* **2011**, *12*, 3174–3185.
17. Ruoslahti, E. RGD and Recognition Sequences for Integrins. *Annu. Rev. Cell Dev. Biol.* **1996**, *12*, 697–715.
18. Xiong, J.; Stehle, T.; Zhang, R.; Joachimiak, A.; Frech, M.; Goodman, S.; Arnaout, M. Crystal Structure of the Extracellular Segment of Integrin $\alpha_v\beta_3$ in Complex with an Arg-Gly-Asp Ligand. *Science* **2002**, *296*, 151–155.
19. Haubner, R.; Gratias, R.; Diefenbach, B.; Goodman, S.; Jonczyk, A.; Kessler, H. Structural and Functional Aspects of RGD-Containing Cyclic Pentapeptides as Highly Potent and Selective Integrin $\alpha_v\beta_3$ Antagonists. *J. Am. Chem. Soc.* **1996**, *118*, 7461–7472.
20. Gladson, C. Expression of Integrin $\alpha_v\beta_3$ in Small Blood Vessels of Glioblastoma Tumors. *J. Neuropath. Exp. Neur.* **1996**, *55*, 1143–1149.
21. Oba, M.; Aoyagi, K.; Miyata, K.; Matsumoto, Y.; Itaka, K.; Nishiyama, N.; Yarnasaki, Y.; Koyama, H.; Kataoka, K. Polyplex Micelles with Cyclic RGD Peptide Ligands and Disulfide Cross-Links Directing to the Enhanced Transfection *via* Controlled Intracellular Trafficking. *Mol. Pharmaceutics* **2008**, *5*, 1080–1092.
22. Meister, A.; Anderson, M. Glutathione. *Annu. Rev. Biochem.* **1983**, *52*, 711–760.
23. Singh, R.; Kats, L.; Blattler, W.; Lambert, J. Formation of N-Substituted 2-Iminothiolanes when Amino Groups in Proteins and Peptides are Modified by 2-Iminothiolane. *Anal. Biochem.* **1996**, *236*, 114–125.
24. Tam, J.; Wu, C.; Liu, W.; Zhang, J. Disulfide Bond Formation in Peptides by Dimethyl Sulfoxide—Scope and Applications. *J. Am. Chem. Soc.* **1991**, *113*, 6657–6662.
25. Kenausis, G.; Voros, J.; Elbert, D.; Huang, N.; Hofer, R.; Ruiz-Taylor, L.; Textor, M.; Hubbell, J.; Spencer, N. Poly(L-lysine)-*g*-Poly(ethylene glycol) Layers on Metal Oxide Surfaces: Attachment Mechanism and Effects of Polymer Architecture on Resistance to Protein Adsorption. *J. Phys. Chem. B* **2000**, *104*, 3298–3309.
26. Oba, M.; Fukushima, S.; Kanayama, N.; Aoyagi, K.; Nishiyama, N.; Koyama, H.; Kataoka, K. Cyclic RGD Peptide-Conjugated Polyplex Micelles as a Targetable Gene Delivery System Directed to Cells Possessing $\alpha_v\beta_3$ and $\alpha_v\beta_5$ Integrins. *Bioconjugate Chem.* **2007**, *18*, 1415–1423.
27. Shayakhmetov, D.; Eberly, A.; Li, Z.; Lieber, A. Deletion of Penton RGD Motifs Affects the Efficiency of Both the Internalization and the Endosorne Escape of Viral Particles Containing Adenovirus Serotype 5 or 35 Fiber Knobs. *J. Virol.* **2005**, *79*, 1053–1061.
28. Lu, J.; Langer, R.; Chen, J. A Novel Mechanism Is Involved in Cationic Lipid-Mediated Functional siRNA Delivery. *Mol. Pharmaceutics* **2009**, *6*, 763–771.
29. Dijkgraaf, I.; Kruijtzer, J.; Liu, S.; Soede, A.; Oyen, W.; Corstens, F.; Liskamp, R.; Boerman, O. Improved Targeting of the $\alpha_v\beta_3$ Integrin by Multimerisation of RGD Peptides. *Eur. J. Nucl. Med. Mol. I* **2007**, *34*, 267–273.
30. Liu, S. Radiolabeled Cyclic RGD Peptides as Integrin $\alpha_v\beta_3$-Targeted Radiotracers: Maximizing Binding Affinity *via* Bivalency. *Bioconjugate Chem.* **2009**, *20*, 2199–2213.
31. Sancey, L.; Garanger, E.; Foillard, S.; Schoehn, G.; Hurbin, A.; Albiges-Rizo, C.; Boturyn, D.; Souchier, C.; Grichine, A.; Dumy, P.; Coll, J. Clustering and Internalization of Integrin $\alpha_v\beta_3$ with a Tetrameric RGD-Synthetic Peptide. *Mol. Ther.* **2009**, *17*, 837–843.
32. Wangler, C.; Maschauer, S.; Prante, O.; Schafer, M.; Schirrmacher, R.; Bartenstein, P.; Eisenhut, M.; Wangler, B. Multimerization of cRGD Peptides by Click Chemistry: Synthetic Strategies, Chemical Limitations, and Influence on Biological Properties. *ChemBioChem* **2010**, *11*, 2168–2181.
33. Wattiaux, R.; Laurent, N.; Wattiaux-De Coninck, S.; Jadot, M. Endosomes, Lysosomes: Their Implication in Gene Transfer. *Adv. Drug Delivery Rev.* **2000**, *41*, 201–8.
34. Alam, M.; Ming, X.; Fisher, M.; Lackey, J.; Rajeev, K.; Manoharan, M.; Juliano, R. Multivalent Cyclic RGD Conjugates for Targeted Delivery of Small Interfering RNA. *Bioconjugate Chem.* **2011**, *22*, 1673–1681.
35. Matsumoto, Y.; Nomoto, T.; Cabral, H.; Matsumoto, Y.; Watanabe, S.; Christie, R. J.; Miyata, K.; Oba, M.; Ogura, T.; Yamasaki, Y.; *et al.* Direct and Instantaneous Observation of Intravenously Injected Substances Using Intravital Confocal Micro-Videography. *Biomed. Opt. Express* **2010**, *1*, 1209–1216.
36. Nomoto, T.; Matsumoto, Y.; Miyata, K.; Oba, M.; Fukushima, S.; Nishiyama, N.; Yamasoba, T.; Kataoka, K. *In Situ* Quantitative Monitoring of Polyplexes and Polyplex Micelles in the Blood Circulation Using Intravital Real-Time Confocal Laser Scanning Microscopy. *J. Controlled Release* **2011**, *151*, 104–109.
37. Choi, H.; Liu, W.; Misra, P.; Tanaka, E.; Zimmer, J.; Ipe, B.; Bawendi, M.; Frangioni, J. Renal Clearance of Quantum Dots. *Nat. Biotechnol.* **2007**, *25*, 1165–1170.
38. Kanda, T.; Sullivan, K.; Wahl, G. Histone-GFP Fusion Protein Enables Sensitive Analysis of Chromosome Dynamics in Living Mammalian Cells. *Curr. Biol.* **1998**, *8*, 377–385.
39. Jin, Z.; Josserand, V.; Foillard, S.; Boturyn, D.; Dumy, P.; Favrot, M.; Coll, J. *In Vivo* Optical Imaging of Integrin $\alpha_v\beta_3$ in Mice Using Multivalent or Monovalent cRGD Targeting Vectors. *Mol. Cancer* **2007**, *6*, 41.
40. Eliceiri, B.; Cheresh, D. The Role of α_v Integrins During Angiogenesis: Insights into Potential Mechanisms of Action and Clinical Development. *J. Clin. Invest.* **1999**, *103*, 1227–1230.
41. Montet, X.; Montet-Abou, K.; Reynolds, F.; Weissleder, R.; Josephson, L. Nanoparticle Imaging of Integrins on Tumor Cells. *Neoplasia* **2006**, *8*, 214–222.
42. Hicklin, D.; Ellis, L. Role of the Vascular Endothelial Growth Factor Pathway in Tumor Growth and Angiogenesis. *J. Clin. Oncol.* **2005**, *23*, 1011–1027.
43. Bergers, G.; Benjamin, L. Tumorigenesis and the Angiogenic Switch. *Nat. Rev. Cancer* **2003**, *3*, 401–410.
44. Schiffelers, R.; Ansari, A.; Xu, J.; Zhou, Q.; Tang, Q.; Storm, G.; Molema, G.; Lu, P.; Scaria, P.; Woodle, M. Cancer siRNA Therapy by Tumor Selective Delivery with Ligand-Targeted Sterically Stabilized Nanoparticle. *Nucleic Acids Res.* **2004**, *32*, e149.
45. Kim, B.; Tang, Q.; Biswas, P.; Xu, J.; Schiffelers, R.; Xie, F.; Ansari, A.; Scaria, P.; Woodle, M.; Lu, P.; Rouse, B. Inhibition of Ocular Angiogenesis by siRNA Targeting Vascular Endothelial Growth Factor Pathway Genes - Therapeutic Strategy for Herpetic Stromal Keratitis. *Am. J. Pathol.* **2004**, *165*, 2177–2185.
46. Kim, J.; Kim, S.; Kim, W. PEI-*g*-PEG-RGD/Small Interference RNA Polyplex-Mediated Silencing of Vascular Endothelial Growth Factor Receptor and Its Potential as an Anti-Angiogenic Tumor Therapeutic Strategy. *Oligonucleotides* **2011**, *21*, 101–107.
47. Ellman, G. Tissue Sulfhydryl Groups. *Arch. Biochem. Biophys.* **1959**, *82*, 70–77.

Journal of Controlled Release 161 (2012) 868–874

Contents lists available at SciVerse ScienceDirect

Journal of Controlled Release

journal homepage: www.elsevier.com/locate/jconrel

Pancreatic cancer therapy by systemic administration of VEGF siRNA contained in calcium phosphate/charge-conversional polymer hybrid nanoparticles

Frederico Pittella [a,b], Kanjiro Miyata [a], Yoshinori Maeda [b], Tomoya Suma [b], Sumiyo Watanabe [a], Qixian Chen [c], R. James Christie [a], Kensuke Osada [c], Nobuhiro Nishiyama [a], Kazunori Kataoka [a,b,c,d,*]

[a] Division of Clinical Biotechnology, Center for Disease Biology and Integrative Medicine, Graduate School of Medicine, The University of Tokyo, 7-3-1 Hongo, Bunkyo-ku, Tokyo 113-0033, Japan
[b] Department of Bioengineering, Graduate School of Engineering, The University of Tokyo, 7-3-1 Hongo, Bunkyo-ku, Tokyo 113-8656, Japan
[c] Department of Materials Engineering, Graduate School of Engineering, The University of Tokyo, 7-3-1 Hongo, Bunkyo-ku, Tokyo 113-8656, Japan
[d] Center for NanoBio Integration, The University of Tokyo, 7-3-1 Hongo, Bunkyo-ku, Tokyo 113-8656, Japan

ARTICLE INFO

Article history:
Received 16 February 2012
Accepted 1 May 2012
Available online 11 May 2012

Keywords:
siRNA
Calcium phosphate
Nanoparticle
VEGF
PEG
Charge-conversional polymer

ABSTRACT

Development of an efficient *in vivo* delivery vehicle of small interfering RNA (siRNA) is the key challenge for successful siRNA-based therapies. In this study, toward systemic delivery of siRNA to solid tumors, a smart polymer/calcium phosphate (CaP)/siRNA hybrid nanoparticle was prepared to feature biocompatibility, reversible stability and endosomal escape functionality using a pH sensitive block copolymer of poly(ethylene glycol) and charge-conversional polymer (PEG-CCP), of which anionic functional groups could be converted to cationic groups in an endosomal acidic condition for facilitated endosomal escape. Nanoparticles were confirmed to be approximately 100 nm in size, narrowly dispersed and spherical. Also, the nanoparticle was highly tolerable in medium containing serum, while releasing the entrapped siRNA in a cytoplasm-mimicking ionic condition, presumably based on the equilibrium between CaP complexes and calcium ions. Further, the nanoparticle showed high gene silencing efficiency in cultured pancreatic cancer cells (BxPC3) without associated cytotoxicity. Ultimately, systemic administration of the nanoparticles carrying vascular endothelium growth factor (VEGF) siRNA led to the significant reduction in the subcutaneous BxPC3 tumor growth, well consistent with the enhanced accumulation of siRNA and the significant VEGF gene silencing (~68%) in the tumor. Thus, the hybrid nanoparticle was demonstrated to be a promising formulation toward siRNA-based cancer therapies.

1. Introduction

Since elucidation of the molecular pathway of ribonucleic acid interference (RNAi) [1], small interfering ribonucleic acid (siRNA) has emerged as a potential therapeutic agent for modulating the production of proteins associated with disease [2,3]. Several clinical trials employing siRNA-based cancer therapies are currently ongoing [3,4]. In many cases, siRNA has been applied with a delivery vehicle to facilitate accumulation within the therapeutic site of activity (cell cytoplasm). Incorporation of siRNA within delivery vehicles is performed to overcome barriers associated with transport of this fragile and highly anionic macromolecule, such as premature degradation by RNases and inefficient cellular internalization. Therefore, development of more effective delivery vehicles is currently a major challenge for improving siRNA therapies.

Calcium phosphate (CaP)-based nanoparticles are a promising siRNA delivery platform because of the fact that CaP is naturally generated in the body (thus well tolerated), and also encapsulates negatively charged molecules during precipitation [5,6]. In this regard, a strategy to control the growth of CaP/siRNA precipitates is essential for their utilization toward systemic delivery applications. Several previous studies, including ours, have developed successful strategies to control nanoparticle size on the order of several tens to one hundred nanometer by coating with poly(ethylene glycol) (PEG)-*b*-polyanions [7–10], PEG-functionalized bisphosphonate [11], lipid bilayer membranes [12], or even nucleic acids [13]. Notably, a PEG shell on the nanoparticle surface has the desirable functionality to reduce non-specific interactions with biomacromolecules in the bloodstream, termed stealth property, for improved pharmacokinetics as well as facilitated accumulation in solid tumors through enhanced permeability and retention (EPR) effect [14–17].

Once internalized by cells via endocytosis, nanoparticles are transported to endosomal compartments ultimately lysosome where they remain until degraded. To overcome the endosomal/lysosomal entrapment of CaP nanoparticles, we developed CaP/polymer hybrid

* Corresponding author at: Division of Clinical Biotechnology, Center for Disease Biology and Integrative Medicine, Graduate School of Medicine, The University of Tokyo, 7-3-1 Hongo, Bunkyo-ku, Tokyo 113-0033, Japan.
E-mail address: kataoka@bmw.t.u-tokyo.ac.jp (K. Kataoka).

0168-3659/$ – see front matter © 2012 Elsevier B.V. All rights reserved.
doi:10.1016/j.jconrel.2012.05.005

nanoparticles containing functionality designed to promote escape from these subcellular compartments. This was achieved using a block copolymer of PEG and an endosome-disrupting polyanion, poly(*N*″-{*N*′-[(*N*-*cis*-aconityl)-2-aminoethyl]-2-aminoethyl}aspartamide) (PAsp(DET-Aco)) [18]. PAsp(DET-Aco) is relatively stable at the extracellular pH of 7.4 but degrades at pH ~5.5 (lysosome pH) by cleavage of *cis*-aconitic amide linkages, thus reverting back to the parent polycation, PAsp(DET). This degradation event results in conversion of the polymer charge from anionic to cationic, and is thus termed a charge-conversional polymer (CCP) (Fig. 1) [19]. PAsp(DET) has been shown to exhibit a distinctive change in the structure of side chains between pH 7.4 and pH 5.5 due to protonation of amino groups, i.e., monoprotonated diaminoethane at pH 7.4 and diprotonated diaminoethane at pH 5.5, allowing pH-selective membrane disruption for efficient endosomal escape of nucleic acids without associated toxicity [20–25]. In addition, PEG-PAsp(DET-Aco) was confirmed to facilitate excellent colloidal dispersion of CaP nanoparticles, while also improving the endosomal escape of siRNA, resulting in efficient gene silencing to cultured pancreatic carcinoma cells (PanC-1) [18].

The present work reports the *in vivo* application of the CaP/block copolymer/siRNA hybrid nanoparticles prepared with PEG-PAsp(DET-Aco) for treatment of subcutaneous pancreatic tumor (BxPC3) models in mice by systemic administration. Removal of free calcium ions from CaP nanoparticle solutions is critical for its systemic administration, as excess calcium ions may induce adverse effects in the bloodstream [32]. Thus nanoparticle solutions were purified by ultrafiltration, and then characterized with non-purified controls in terms of stability, morphology, calcium amount and biological activity. For treatment of subcutaneous pancreatic tumors, the key pro-angiogenic molecule vascular endothelial growth factor (VEGF) was selected as the target gene, once it is known to be over-expressed in many cancerous cells, promoting angiogenesis through endothelial proliferation, survival and migration [26]. Moreover, silencing of the VEGF signaling pathway has been shown to suppress tumor angiogenesis and growth [27–30]. After systemic administration of purified nanoparticles incorporating VEGF siRNA for anti-angiogenic therapy, the accumulation of siRNA and the expression level of VEGF mRNA in the tumor tissue were evaluated to elucidate their correlation with tumor growth rates. This work demonstrates significant antitumor activity induced by VEGF gene silencing with siRNA delivered by CaP/block copolymer hybrid nanoparticles.

2. Materials and methods

2.1. Materials, cell line and animals

Dulbecco's modified eagle's medium (DMEM) without L-glutamine and phenol red, RPMI 1640 and *cis*-aconitic anhydride were purchased from Sigma-Aldrich (St. Louis, MO). α-Methoxy-ω-amino poly(ethylene glycol) (MeO–PEG–NH_2) (M_w: 12,000) and β-benzyl-L-aspartate *N*-carboxy anhydride (BLA-NCA) were obtained from NOF Co., Inc. (Tokyo, Japan) and Chuo Kaseihin Co., Inc. (Tokyo, Japan), respectively. *N*-methyl-2-pyrrolidone (NMP), diethylenetriamine (DET), dimethyl sulfoxide (DMSO), *N*,*N*-dimethylformamide (DMF), dichloromethane (DCM) and acetic anhydride were purchased from Tokyo Chemical Industry Co. Ltd. (Tokyo, Japan) or Nacalai Tesque (Tokyo, Japan), and used after conventional distillation. Acetic acid, acetonitrile, acetone, diethyl ether and hydrochloric acid were purchased from Wako Pure Chemical Industries Ltd. (Osaka, Japan). Fetal bovine serum (FBS) was purchased from Dainippon Sumitomo Pharma Co., Ltd. (Osaka, Japan). RT-PCR primers used for human actin and human VEGF were synthesized by Hokkaido System Science (Hokkaido, Japan) and the sequences are the following: CCAACCGCGAGAAGATGA (actin forward); CCAGAGGCGTACAGGGATAG (actin reverse); AGTGGTCCCAGGCTGCAC (VEGF forward); TCCATGAACTTCACCACTTCGT (VEGF reverse). All the siRNAs were synthesized by Hokkaido System Science (Hokkaido, Japan). The sequences of VEGF siRNA (siVEGF) are 5′-GGAGUACCCUGAUGAGAUCdTdT-3′ (sense) and 5′-GAUCUCAUCAGGGUACUCCdTdT-3′ (antisense), and the sequences of scramble siRNA (siSCR) are 5′-UUCUCCGAACGUGUCACGUdTdT-3′ (sense); 5′-ACGUGACACGUUCGGAGAAdTdT-3′ (antisense).

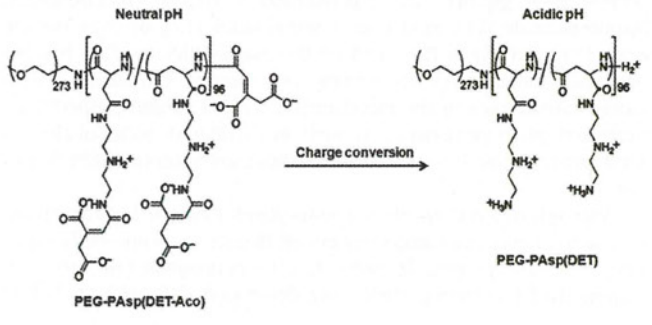

Fig. 1. Change in the chemical structure of PEG-PAsp(DET-Aco) to PEG-PAsp(DET) in response to the acidic pH.

BxPC3 cells (human tumorigenic pancreatic adenocarcinoma, ATCC number: CRL-1687) were obtained from the American Type Culture Collection (Manassas, VA). Cells were maintained in RPMI 1640 medium (Sigma Chemical Co., Inc.) containing 10% fetal bovine serum (FBS) in a humidified atmosphere containing 5% CO_2 at 37 °C. Balb-c nu/nu mice (female; 18–20 g body weight; age, 6 weeks) were purchased from Charles River Japan (Kanagawa, Japan). All animal experiments were performed in accordance with the Guidelines for the Care and Use of Laboratory Animals as stated by the University of Tokyo.

2.2. Polymer synthesis

Detailed synthesis methods of the parent polycation PEG-PAsp(DET) and PEG-PAsp(DET-Aco) derivative are described in Supplementary data.

2.3. Preparation of PEG-CCP/siRNA/CaP hybrid nanoparticles

A solution of 2.5 M $CaCl_2$ (1 μL) was diluted in 10 mM Tris buffer (pH 10) (11.5 μL). Another solution containing PEG-PAsp(DET-Aco) (1.0 mg/mL) in 10 mM Tris/HCl buffer (pH 7.5) was mixed with a solution of 15 μM siRNA in 10 mM HEPES buffer (pH 7.2) and with 50 mM HEPES buffer containing 1.5 mM Na_3PO_4 and 140 mM NaCl (pH 7.5) (2.5 μL: 5 μL: 5 μL). The former solution was mixed with the latter solution by pipetting for around 20 s (final siRNA concentration; 3 μM).

2.4. Purification of PEG-CCP/siRNA/CaP hybrid nanoparticles

The purification of hybrid nanoparticles for removal of excess amount of free calcium ions was carried out immediately after preparation. PEG-CCP/siRNA/CaP hybrid nanoparticle solution containing 41.3 μg siRNA and 150 μg PEG-CCP (1 mL) was added to a VivaSpin-06 device (MWCO: 10 kDa) containing 1 mL of an extracellular (EC) buffer that mimics the ionic strength of extracellular environment (2 mM $CaCl_2$, 1 mM Na_2HPO_4, 25 mM Tris and 140 mM NaCl at pH 7.4) [8]. The mixture was centrifuged in a swing bucket rotor at 900 g and 4 °C for 20 min. To minimize non-specific binding of nanoparticles to the membrane, the centrifuge filter devices were washed with de-ionized water before use. After centrifugation, the retained solution was collected and used in further experiments.

2.5. Determination of calcium content in nanoparticles

The total calcium content present in the solution of non-purified and purified/concentrated hybrid nanoparticles was determined by the SRL Laboratories (SRL Inc., Tokyo, Japan) through spectrophotometry using

arsenazo III. All the samples were diluted four times with distilled water to the final volume of 300 μL before assay. The reaction of arsenazo III dye with calcium under acidic conditions produces a blue–purple complex, of which concentration is determined spectrophotometrically at the wavelength of 660 nm. Obtained values were used to calculate the efficiency of calcium removal from nanoparticle solution.

2.6. Dynamic light scattering (DLS) measurements

DLS measurements were carried out at 25 °C using a Zetasizer Nano ZS (Malvern Instruments, UK) at a detection angle of 173° with a He–Ne laser (633 nm) as the incident beam. The data obtained from the rate of decay in the photon correlation function were analyzed with a cumulant method to obtain the corresponding hydrodynamic diameters and polydispersity indices (PdI) (μ/G^2) of the nanoparticles. The colloidal stability of both purified and non-purified nanoparticles was monitored during several days and the result was presented as a relative size to the initial hydrodynamic diameter obtained in the first day.

2.7. Atomic force microscopy (AFM) imaging

AFM imaging of the nanoparticles was performed using a MMAFM, Nanoscope V (Bruker AXS, Madison, WI) in ScanAsyst Atomic Force Microscopy Imaging mode with standard silicon probes. Imaging was conducted under air on a highly orientated pyrolytic graphite (HOPG) substrate. The obtained images were processed by flattening to remove the background slope of the substrate surface.

2.8. Fluorescence correlation spectroscopy (FCS) measurements

FCS measurements were performed using a Confocor3 module (Carl Zeiss, Jena, Germany) equipped with a Zeiss C-Apochromat 40× water objective. Samples prepared with Cy5-labeled siRNA were measured with the excitation of a He–Ne laser (633 nm, 5 mW) and the emission passed through a 650 nm long pass filter. Samples were placed into 8-well Lab-Tek chambered borosilicate cover-glass slides (Nalge Nunc International, Rochester, NY). Determination of the focal volume was established by calibration with 10 nM Cy5 standard solution. Each analysis consisted of 10 measurements with a sampling time of 20 s and the measured autocorrelation curves were fitted with the Zeiss Confocor3 software package to obtain the diffusion coefficient. The stability of nanoparticles under a cell culture condition was evaluated after dilution of samples with DMEM containing 10% FBS without L-glutamine and phenol red and then incubation at 37 °C. The stability of nanoparticles in the solution mimicking the intracellular fluids was evaluated after dilution of the samples with the ionic solution ($CaCl_2$ 100 nM, Na_2HPO_4 40 mM, NaCl 140 mM, pH 7.4), as previously described [8]. The concentration of Cy5-labeled siRNA was adjusted to 100 nM, corresponding to the *in vitro* gene silencing experiment.

2.9. In vitro gene silencing

To evaluate the gene silencing efficiency of the purified nanoparticles compared to non-purified controls, BxPC3 cells were seeded with 2 mL of RPMI 1640 containing 10% FBS on a 6 well plate at 5×10^4 cells/well. After 24 h, nanoparticle solutions were added with fresh medium (100 nM siRNA). After another 24 h, cells were harvested and RNA was extracted using RNeasy Mini Kit (Qiagen, Valencia, CA), according to the manufacturer's instruction.

2.10. Real-time reverse transcriptional (RT)-PCR

After obtaining the RNA from cells or tissue, the RNA concentration was measured and then sample concentrations were normalized. Next, the genomic DNA elimination was performed prior to cDNA synthesis using a QuantiTect Reverse Transcription kit (Qiagen, Valencia, CA). Real-time RT-PCR was performed using an ABI 7500 Fast Real-time RT-PCR System (Applied Biosystems, Foster City, CA) and QuantiTect SYBR Green PCR Master Mix (Qiagen, Valencia, CA). Actin was used as the house-keeper gene and the obtained data were normalized before statistical analysis.

2.11. Antitumor activity

Balb/c nude mice (female, 6 week old) were subcutaneously implanted with BxPC3 tumor (3 mm × 3 mm × 1 mm). The tumors were allowed to grow for 3 weeks before sample injection. Further, the mice bearing tumors with similar volume (~50 mm^3) were randomly distributed in groups ($n = 4$). Thereafter, hybrid nanoparticles loading siVEGF (25 μg siRNA in 200 μL per injection) were injected into the tail vein 4 times at days 2, 5, 8 and 12. Tumor size and body weight for each mouse were monitored for 13 days. The tumor volume was calculated based on a modified ellipsoidal formula [30,31]: tumor volume $= 1/2(\text{length} \times \text{width}^2)$.

2.12. Tumor accumulation

Similarly to Section 2.11, BxPC3 tumor-bearing mice were prepared by subcutaneous implantation of the tumor pieces (3 mm × 3 mm × 1 mm). The tumors were allowed to grow for 4 weeks before sample injection. Five mice bearing tumors of the similar volume (~70 mm^3) were randomly selected for each cohort ($n = 5$). Hybrid nanoparticles containing Cy5-labeled siRNA were intravenously injected into the tail vein at 15 μg of Cy5-labeled siRNA per injection. Mice were sacrificed 60 min after injection and tumors were excised. Cy5 fluorescence from the tumor tissue was measured by IVIS (Caliper Life Sciences, Hopkinton, MA). Results were expressed as total photon counts normalized by tumor weight.

2.13. In vivo gene silencing in tumor tissue

BxPC3 tumor-bearing mice were prepared by subcutaneous implantation of the tumor pieces (3 mm × 3 mm × 1 mm) and then allowed to grow for 4 weeks, similar to the method described in Sections 2.11 and 2.12. Mice bearing tumors of similar volume (~70 mm^3) were randomly distributed in groups ($n = 3$). Thereafter, hybrid nanoparticles loading siVEGF (25 μg siRNA in 200 μL per injection) were injected into the tail vein on days 1, 4, 8 and 34. After 24 h of the last injection, each tumor was excised and the non-necrotic part of the tumor (~20 mg) was cut into small pieces and sonicated for 10 s in a lysis buffer. The lysate was centrifuged and then the supernatant was used to extract RNA using the RNeasy Mini Kit (Qiagen, Valencia, CA), according to the manufacturer's instruction. Extracted RNA was further used to verify VEGF gene silencing by real-time RT-PCR, as described in Section 2.10.

3. Results and discussion

3.1. Preparation and purification/concentration of hybrid nanoparticles

The functional CCP block copolymer, PEG-PAsp(DET-Aco) (Fig. 1), was synthesized using a procedure similar to our previous report [18]. Successful synthesis of PEG-PAsp(DET-Aco) was confirmed from the ^{1}H NMR spectrum (Supporting Fig. 1) by the appearance of protons present on acid-labile *cis*-aconitic amide (Aco) moieties. This introduction is accompanied by the conversion of cationic charges to negative charges in the polyaspartamide side chain, enabling integration of PEG-CCP into CaP nanoparticles. The prepared charge-conversional polymer shows high stability at neutral pH but becomes cleavable at acidic pH to reproduce cationic PAsp(DET) from anionic PAsp(DET-Aco) (Fig. 1). Note that, once in the acidic environment of the endosome/lysosome, PAsp(DET) can disrupt their membrane to facilitate the escape of nanoparticles from these compartments [18,25].

PEG-CCP/CaP hybrid nanoparticles were prepared by simple mixing of the component solutions [18]. The initial solution of the prepared nanoparticles contains several ions, such as Ca^{2+}, that may perturb the normal body homeostasis when applied systemically [32], thereby requiring purification of the solution for removal of the ions before systemic administration. However, the CaP nanoparticles are likely to dissociate in lower ionic strength solutions due to an equilibrium shift [8–10]. Thus, a suitable buffer solution is necessary for maintaining nanoparticle structure after purification. Our previous work suggested that PEGylated CaP nanoparticles were tolerable to an extracellular ionic solution ($CaCl_2$ 2 mM, Na_2HPO_4 1 mM, Tris 25 mM, NaCl 140 mM, pH 7.4) as they effectively delivered siRNA into cultured cells in that solution. The calcium concentration of the extracellular ionic solution is similar to that of body fluids, suggesting that minimal perturbation to blood homeostasis following intravenous administration is expected.

Hybrid nanoparticle solutions were purified by an ultrafiltration method, which allows rapid exchange of the buffer solutions. The ultrafiltration (MWCO: 10 kDa) was performed with replacement of the original solution for nanoparticle preparation ($CaCl_2$ 100 mM, Na_3PO_4 0.3 mM, NaCl 28 mM, Tris 6.6 mM, HEPES 12 mM) with EC buffer ($CaCl_2$ 2 mM, Na_2HPO_4 1 mM, Tris 25 mM, NaCl 140 mM, pH 7.4). The arsenazo III dye-based colorimetric assay revealed that the ultrafiltration process removed 84% of the original calcium content, with residual calcium corresponding mostly to the calcium contained in nanoparticles. The resulting nanoparticles were characterized by DLS and AFM. Purified nanoparticles maintained a narrowly dispersed size distribution in the DLS (Z-weighted) histogram, similar to non-purified controls (Fig. 2A). Spherical morphologies with the similar size were observed in the AFM images of both purified and non-purified hybrid nanoparticles (Figs. 2B and C). These results indicate that purification for removal of excess calcium ions was successful, without alteration of hybrid nanoparticle structure.

Hybrid nanoparticle stability upon storage is also important for their quality control towards pharmaceutical applications. Thus, the size of hybrid nanoparticle was monitored over time by DLS following storage at 4 °C (Fig. 3). Non-purified hybrid nanoparticles did not show a significant change in both size and PdI for at least 168 h (7 days). Purified nanoparticle size remained similar to that of the non-purified control for the first 96 h and then the size slightly increased thereafter, possibly due to secondary aggregate formation. This aggregation can be explained by compromised colloidal stability of nanoparticles, triggered by PEG-CCP detachment from the nanoparticles associated with their gradual dissolution. These results suggest that the dissolution of the purified nanoparticle is intrinsically slow in the EC buffer.

3.2. Stability of hybrid nanoparticles in a serum-containing culture medium and a cytoplasmic ionic solution

Purified hybrid nanoparticle stability was further assessed in medium containing serum proteins. Nanoparticles were prepared with Cy5-labeled siRNA (Cy5-siRNA) and then subjected to fluorescence correlation spectroscopy (FCS) analysis. FCS analysis allows determination of the diffusion coefficient of siRNA-incorporating nanoparticles in the complex protein-containing solution without interference from non-labeled macromolecules or aggregates [33–35]. Note that the diffusion coefficient is inversely proportional to the hydrodynamic size of the fluorescent molecule based on the Stokes–Einstein equation for spherical particles; thus the size of nanoparticles can be determined. In conventional condition used for siRNA transfection (100 nM siRNA in 10% FBS medium), the initial size of nanoparticles was determined to be approximately 100 nm (Fig. 4A), which is consistent with the size in DLS histogram and AFM image of nanoparticles not exposed to biological media (Fig. 2). Additionally, size was maintained following 4 h incubation at 37 °C, indicating high tolerability in medium containing serum proteins.

In addition to high tolerability within extracellular conditions, delivery vehicles must finally release the encapsulated siRNA in the cytoplasm to gain access to the RNAi pathway. Hence, siRNA release from the hybrid nanoparticles was further evaluated by FCS in a solution mimicking the ionic condition of the cytoplasm ($CaCl_2$ 100 nM, Na_2HPO_4 40 mM, NaCl 140 mM, pH 7.4), as the dissolution of CaP nanoparticles should be significantly influenced by the concentration of calcium and phosphate ions. The average calcium ion concentrations are 2 mM and 100 nM in the blood and the cytoplasm, respectively. The lower calcium concentration in the cell cytoplasm may trigger selective intracellular release of siRNA from the CaP nanoparticles. Indeed, when nanoparticles were incubated in the cytoplasmic ionic solution, the size of the nanoparticles was drastically reduced within 1 h incubation, ultimately reaching the same value of naked siRNA (Fig. 4B), which is consistent with our previous findings regarding the dissolution behavior of hybrid nanoparticles [8].

3.3. In vitro gene silencing

The gene silencing activity of nanoparticles containing siVEGF was evaluated in cultured human pancreatic adenocarcinoma (BxPC3) cells. BxPC3 was chosen as a target cancer cell because of the fact that subcutaneous BxPC3 tumors exhibit poorly differentiated histology with thick fibrotic stromal tissue surrounding tumor nests [36], thereby resembling intractable tumors in clinical settings. As shown in Fig. 5, both non-purified and purified hybrid nanoparticles encapsulating siVEGF significantly reduced VEGF mRNA in comparison with controls incorporating siSCR. The reduction in VEGF mRNA was 71% and 63% for purified and non-purified nanoparticles, respectively. Strong gene silencing activity of hybrid nanoparticles is probably due to their high complex stability in the transfection medium (Fig. 4A) and selective siRNA release in the cell cytoplasm (Fig. 4B) as well as facilitated endosomal escape of siRNA by PEG-CCP, as extensively examined in previous studies [18,19]. No statistical difference was found between nanoparticle formulations, indicating that there was apparently no loss of the biological activity of siRNA after purification. Analysis of cell viability (CCK-8, Dojindo, Japan) showed no difference between nanoparticle-treated samples and controls at tested siRNA

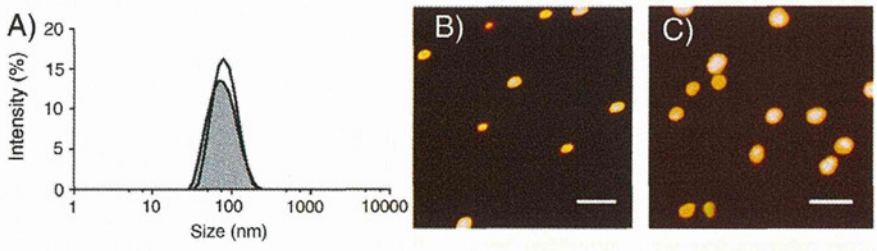

Fig. 2. (A) Size distribution of CaP nanoparticles before (filled curve) and after (open curve) purification by ultrafiltration, determined by DLS. (B, C) Atomic force microscopic images of non-purified (B) and purified (C) hybrid nanoparticles. Scale bar corresponds to 200 nm.

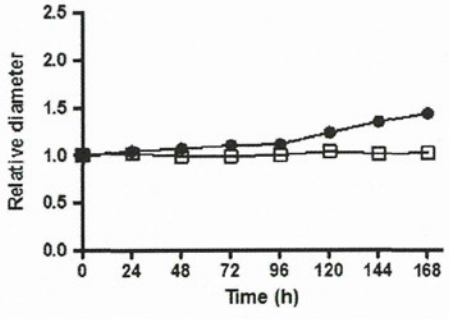

Fig. 3. Time-dependent change in the relative diameter of non-purified (open square) and purified (closed circle) hybrid nanoparticles, determined by DLS (temperature: 4 °C, siRNA concentration: 3 μM).

concentration (Supporting Fig. 2), indicating that VEGF silencing is due to the RNAi effect and not an artifact of toxicity.

3.4. Antitumor activity

Antitumor activity of siVEGF-incorporating hybrid nanoparticles was evaluated against a subcutaneous BxPC3 tumor model. Silencing of VEGF gene in tumor tissues can prevent angiogenesis, subsequently blocking the nutrient supply needed for tumor growth (antiangiogenic therapy). As presented in Fig. 6, tumors treated by I.V. injection of nanoparticles containing siVEGF showed suppressed growth, compared to those treated with nanoparticles containing siSCR as well as nanoparticles without siRNA and EC buffer only. A statistical significance was observed at days 3, 5, 7 and 9 for tumors treated with the siVEGF nanoparticles compared to controls. It is noteworthy that the significant tumor growth inhibition was observed after the first injection of the siVEGF nanoparticle. At day 9, the tumor volume in mice treated with the siVEGF nanoparticles was around 66% of the average volume of controls. I.V. injection of nanoparticles did not result in

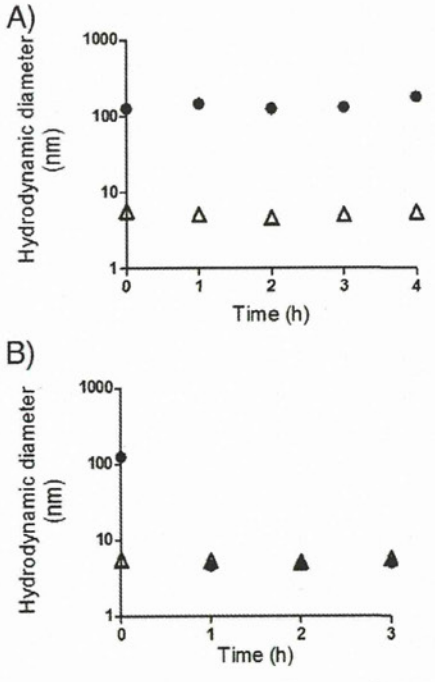

Fig. 4. Time-dependent change in hydrodynamic diameters of hybrid nanoparticles incorporating Cy5-siRNA (closed circle) and naked Cy5-siRNA (open triangle) determined by FCS in the medium containing 10% FBS (A) and in the medium mimicking the cytoplasm (Ca^{2+} and PO_4^{3-} concentrations were 100 nM and 40 mM, respectively) (B).

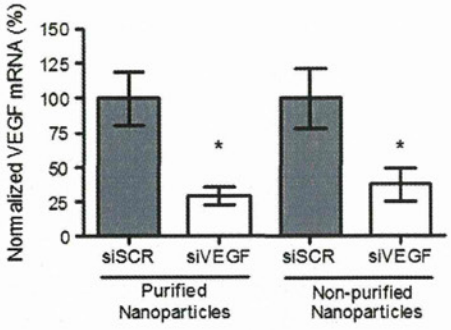

Fig. 5. Gene silencing activity of hybrid nanoparticles in cultured BxPC3 cells (siRNA concentration: 100 nM, incubation time: 24 h, $n=3$). *$p<0.05$ for the control incorporating siSCR (ANOVA followed by Newman–Keuls).

acute or severe toxicity, as no significant difference in body weight was observed between treated and control groups during the experimental period (data not shown). Additionally, blood levels of alanine aminotransferase (ALT) and aspartate aminotransferase (AST) were not significantly altered after I.V. injection of hybrid nanoparticles (Supporting Fig. 3), suggesting negligible acute toxicity associated with nanoparticle administration. These results demonstrate that the PEG-CCP/CaP hybrid nanoparticle with siVEGF is a promising formulation for cancer therapy.

3.5. Accumulation of siRNA and gene silencing in tumors

In order to obtain further evidence that the antitumor activity of siRNA-containing hybrid nanoparticles was induced by the RNAi effect, accumulation of siRNA within subcutaneous tumors was evaluated. Hybrid nanoparticles were prepared with Cy5-siRNA and injected into mice in the similar manner used for tumor growth inhibition experiments. Mice were sacrificed and the tumors were excised 60 min after systemic administration of the hybrid nanoparticles, and Cy5 fluorescence was measured by *IVIS*. Fluorescence intensity was normalized to the tumor weight for quantitative evaluation. Significantly stronger fluorescence was detected in tumors treated with hybrid nanoparticles, compared to naked siRNA (Fig. 7A), indicating enhanced tumor accumulation of siRNA by hybrid nanoparticle delivery. Considering the fact that naked siRNA is immediately degraded in the bloodstream and subsequently cleared from kidney, the improved tumor accumulation may be due to suppressed siRNA degradation in the bloodstream as well as slower renal clearance of siRNA.

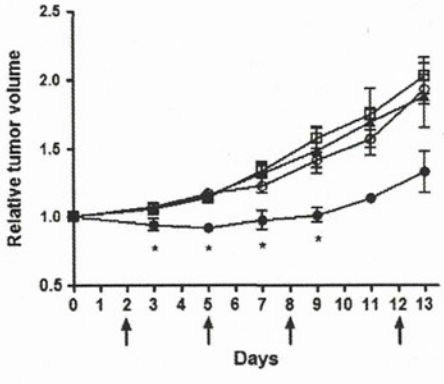

Fig. 6. Relative tumor volume of subcutaneous BxPC3 tumors treated by the hybrid nanoparticles with siVEGF (closed circle), with siSCR (closed triangle), hybrid nanoparticles without siRNA (open square) and EC buffer control (open circle) ($n=4$). Arrows indicate injection day (25 μg siRNA/injection). *$p<0.05$ for EC buffer control (ANOVA followed by Newman–Keuls).

Target gene mRNA levels were also evaluated as direct evidence for RNAi-based antitumor activity. In order to confirm VEGF mRNA degradation in tumor tissue, an additional injection of nanoparticles was performed to a separated group of mice bearing subcutaneous BxPC3 tumors ($n=3$). Approximately 1 day after the injection, mice were sacrificed and tumors were excised, followed by the extraction of RNA and real-time RT-PCR analysis. Fig. 7B clearly shows that significantly higher gene silencing activity (~68%) was achieved with hybrid nanoparticles containing siVEGF, compared to those prepared with siSCR as well as a buffer control. This result corroborates with the significant antitumor activity achieved with nanoparticles containing siVEGF (Fig. 6). Altogether, effective tumor accumulation and VEGF mRNA degradation strongly suggest that tumor growth suppression was a result of RNAi.

4. Conclusion

In this work, the *in vivo* application of PEG-CCP/CaP hybrid nanoparticles carrying siRNA was investigated for siRNA-based cancer treatment. Hybrid nanoparticles were submitted to purification for significant reduction of the amount of free calcium in solution. Purified hybrid nanoparticles were found to have the following characteristics: i) a similar size distribution and morphology to non-purified controls, ii) excellent tolerability in the serum-containing medium, iii) reversible capture of siRNA, with release in cytoplasmic ionic conditions. Efficient gene silencing activity without associated toxicity was also confirmed for nanoparticles in cultured BxPC3 cells. Intravenously injected nanoparticles incorporating VEGF siRNA led to significant reduction in tumor growth. Enhanced siRNA accumulation in subcutaneous BxPC3 tumors was found and subsequently induction of effective VEGF gene silencing in the tumor was observed. Based on the presented results, the PEG-CCP/CaP hybrid nanoparticles demonstrate great potential for clinical applications toward siRNA-based cancer therapies.

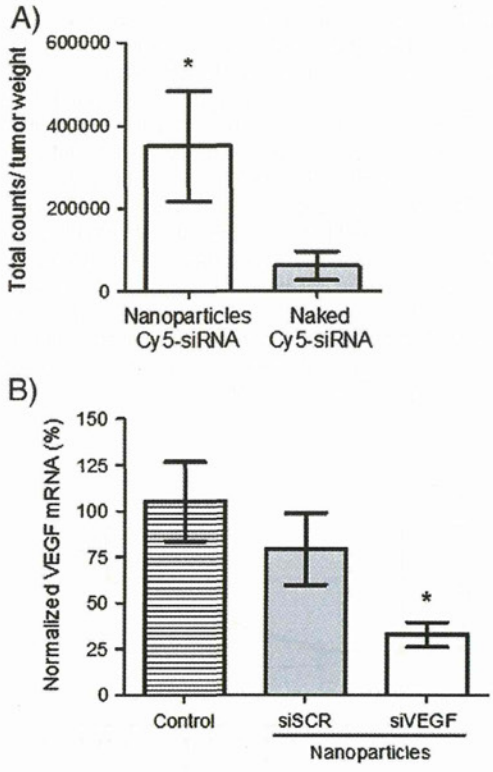

Fig. 7. (A) Accumulation of Cy5-siRNA in subcutaneous BxPC3 tumors 60 min after systemic administration. The Cy5 fluorescence intensity in the excised tumor tissue was determined by IVIS, followed by the normalization by the tumor weight ($n=5$). *$p<0.05$ for naked Cy5-siRNA (Mann–Whitney t test). (B) *In vivo* VEGF gene silencing activity in subcutaneous BxPC3 tumors 1 day after systemic administration of samples (25 μg siRNA), revealed by real-time RT-PCR ($n=3$). *$p<0.05$ for ionic buffer control (ANOVA followed by Newman–Keuls).

Acknowledgment

This research was granted by the Japan Society for the Promotion of Science (JSPS) through the "Funding Program for World-Leading Innovative R&D on Science and Technology (FIRST Program)," initiated by the Council for Science and Technology Policy (CSTP). The authors express their appreciation to Dr. M. Oba (Nagasaki University) and Dr. H. Cabral (The University of Tokyo) for the help in animal experiments.

Appendix A. Supplementary data

Supplementary data to this article can be found online at http://dx.doi.org/10.1016/j.jconrel.2012.05.005.

References

[1] A. Fire, S. Xu, M.K. Montgomery, S.A. Kostas, S.E. Driver, C.C. Mello, Potent and specific genetic interference by double-stranded RNA in *Caenorhabditis elegans*, Nature 391 (1998) 806–811.
[2] S.M. Elbashir, J. Harborth, W. Lendeckel, A. Yalcin, K. Weber, T. Tushl, Duplexes of 21-nucleotide RNAs mediate interference in cultured mammalian cells, Nature 411 (2001) 494–498.
[3] B.L. Davidson, P.B. McCray, Current prospects for RNA interference-based therapies, Nat. Rev. Genet. 12 (2011) 329–340.
[4] M.E. Davis, J.E. Zuckerman, C.H.J. Choi, D. Seligson, A. Tolcher, C.A. Alabi, Y. Yen, J.D. Heidel, A. Ribas, Evidence of RNAi in humans from systemically administered siRNA via targeted nanoparticles, Nature 464 (2010) 1067–1070.
[5] A. Maitra, Calcium phosphate nanoparticles: second-generation nonviral vectors in gene therapy, Expert. Rev. Mol. Diagn. 5 (2005) 893–905.
[6] M. Zhang, K. Kataoka, Nano-structured composites based on calcium phosphate for cellular delivery of therapeutic and diagnostic agents, Nano Today 4 (2009) 508–517.
[7] Y. Kakizawa, K. Kataoka, Block copolymer self-assembly into monodispersive nanoparticles with hybrid core of antisense DNA and calcium phosphate, Langmuir 18 (2002) 4539–4543.
[8] Y. Kakizawa, S. Furukawa, K. Kataoka, Block copolymer-coated calcium phosphate nanoparticles sensing intracellular environment for oligodeoxynucleotide and siRNA delivery, J. Control. Release 97 (2004) 345–356.
[9] Y. Kakizawa, S. Furukawa, A. Ishii, K. Kataoka, Organic–inorganic hybrid-nanocarrier of siRNA constructing through the self-assembly of calcium phosphate and PEG-based block aniomer, J. Control. Release 111 (2006) 368–370.
[10] M. Zhang, A. Ishii, N. Nishiyama, S. Matsumoto, T. Ishii, Y. Yamasaki, K. Kataoka, PEGylated calcium phosphate nanocomposites as smart environment-sensitive carriers for siRNA delivery, Adv. Mater. 21 (2009) 3520–3525.
[11] E.V. Giger, J. Puigmartí-Luis, R. Schlatter, B. Castagner, P.S. Dittrich, J.C. Leroux, Gene delivery with bisphosphonate-stabilized calcium phosphate nanoparticles, J. Control. Release 150 (2011) 87–93.
[12] J. Li, Y.C. Chen, Y.C. Tseng, C. Mozumdar, L. Huang, Biodegradable calcium phosphate nanoparticle with lipid coating for systemic siRNA delivery, J. Control. Release 142 (2010) 416–421.
[13] V.V. Sokolova, I. Radtke, R. Heumann, M. Epple, Effective transfection of cells with multi-shell calcium phosphate DNA nanoparticles, Biomaterials 27 (2006) 3147–3153.
[14] Y. Matsumura, H. Maeda, A new concept for macromolecular therapeutics in cancer-chemotherapy: mechanisms of tumoritropic accumulation of proteins and the antitumor agent SMANCS, Cancer Res. 46 (1986) 6387–6392.
[15] S.M. Moghimi, A.C. Hunter, J.C. Murray, Long-circulating and target-specific nanoparticles: theory to practice, Pharm. Rev. 53 (2001) 283–318.
[16] K. Kataoka, A. Harada, Y. Nagasaki, Block copolymer micelles for drug delivery: design, characterization and biological significance, Adv. Drug Deliv. Rev. 47 (2001) 113–131.
[17] K. Miyata, R.J. Christie, K. Kataoka, Polymeric micelles for nano-scale drug delivery, React. Funct. Polym. 71 (2011) 227–234.
[18] F. Pittella, M. Zhang, Y. Lee, H.J. Kim, T. Tockary, K. Osada, T. Ishii, K. Miyata, N. Nishiyama, K. Kataoka, Enhanced endosomal escape of siRNA-incorporating hybrid nanoparticles from calcium phosphate and PEG-block charge-conversional polymer for efficient gene knockdown with negligible cytotoxicity, Biomaterials 32 (2011) 3106–3114.
[19] Y. Lee, K. Miyata, M. Oba, T. Ishii, S. Fukushima, M. Han, H. Koyama, N. Nishiyama, K. Kataoka, Charge-conversional ternary polyplex with endosome disruption moiety: a technique for efficient and safe gene delivery, Angew. Chem. Int. Ed. 47 (2008) 5163–5166.
[20] N. Kanayama, S. Fukushima, N. Nishiyama, K. Itaka, W.D. Jang, K. Miyata, Y. Yamasaki, U.I. Chung, K. Kataoka, A PEG-based biocompatible block catiomer with high buffering capacity for the construction of polyplex micelles

showing efficient gene transfer toward primary cells, ChemMedChem 1 (2006) 439–444.
[21] K. Miyata, M. Oba, M. Nakanishi, S. Fukushima, Y. Yamasaki, H. Koyama, N. Nishiyama, K. Kataoka, Polyplexes from poly(aspartamide) bearing 1,2-diaminoethane side chains induce pH-selective, endosomal membrane destabilization with amplified transfection and negligible cytotoxicity, J. Am. Chem. Soc. 130 (2008) 16287–16294.
[22] S. Takae, K. Miyata, M. Oba, T. Ishii, N. Nishiyama, K. Itaka, Y. Yamasaki, H. Koyama, K. Kataoka, PEG-detachable polyplex micelles based on disulfide-linked block catiomers as bioresponsive nonviral gene vectors, J. Am. Chem. Soc. 130 (2008) 6001–6009.
[23] K. Itaka, T. Ishii, Y. Hasegawa, K. Kataoka, Biodegradable polyamino acid-based polycations as safe and effective gene carrier minimizing cumulative toxicity, Biomaterials 31 (2010) 3707–3714.
[24] H. Uchida, K. Miyata, M. Oba, T. Ishii, T. Suma, K. Itaka, N. Nishiyama, K. Kataoka, Odd-even effect of repeating aminoethylene units in the side chain of N-substituted polyaspartamides on gene transfection profiles, J. Am. Chem. Soc. 133 (2011) 15524–15532.
[25] K. Miyata, N. Nishiyama, K. Kataoka, Rational design of smart supramolecular assemblies for gene delivery: chemical challenge in the creation of artificial viruses, Chem. Soc. Rev. 41 (2012) 2562–2574.
[26] N. Ferrara, VEGF as a therapeutic target in cancer, Oncology 69 (2005) 11–16.
[27] Y. Takei, K. Kadomatsu, Y. Yuzawa, S. Matsuno, T. Muramatsu, A small interfering RNA targeting vascular endothelial growth factor as cancer therapeutics, Cancer Res. 64 (2004) 3365–3370.
[28] E. Song, P. Zhu, S.K. Lee, D. Chowdhury, S. Kussman, D.M. Dykxhoorn, Y. Feng, D. Palliser, D.B. Weiner, P. Shankar, W.A. Marasco, J. Lieberman, Antibody mediated in vivo delivery of small interfering RNAs via cell-surface receptors, Nat. Biotechnol. 23 (2005) 709–717.
[29] W.J. Kim, L.V. Christensen, S. Jo, J.W. Yockman, J.H. Jeong, Y.H. Kim, S.W. Kim, Cholesteryl oligoarginine delivering vascular endothelial growth factor siRNA effectively inhibits tumor growth in colon adenocarcinoma, Mol. Ther. 14 (2006) 343–350.
[30] H.J. Kim, M. Oba, F. Pittella, T. Nomoto, H. Cabral, Y. Matsumoto, K. Miyata, N. Nishiyama, K. Kataoka, PEG-detachable cationic polyaspartamide derivatives bearing stearoyl moieties for systemic siRNA delivery toward subcutaneous BxPC3 pancreatic tumor, J. Drug Target. 20 (2012) 33–42.
[31] D.M. Euhus, C. Hudd, M.C. LaRegina, F.E. Johnson, Tumor measurement in the nude mouse, J. Surg. Oncol. 31 (1986) 229–234.
[32] A.W. Winkler, H.E. Hoff, P.K. Smith, Cardiovascular effects of potassium, calcium, magnesium, and barium: an experimental study of toxicity and rationale of use in therapeutics, Yale J. Biol. Med. 13 (1940) 123–132.
[33] K. Buyens, M. Meyer, E. Wagner, J. Demeester, S.C.D. Smedt, N.N. Sanders, Monitoring the disassembly of siRNA polyplexes in serum is crucial for predicting their biological efficacy, J. Control. Release 141 (2010) 38–41.
[34] H.J. Kim, A. Ishii, K. Miyata, Y. Lee, S. Wu, M. Oba, N. Nishiyama, K. Kataoka, Introduction of stearoyl moieties into a biocompatible cationic polyaspartamide derivative, PAsp(DET), with endosomal escaping function for enhanced siRNA-mediated gene knockdown, J. Control. Release 145 (2010) 141–148.
[35] H. Takemoto, A. Ishii, K. Miyata, M. Nakanishi, M. Oba, T. Ishii, Y. Yamasaki, N. Nishiyama, K. Kataoka, Polyion complex stability and gene silencing efficiency with a siRNA-grafted polymer delivery system, Biomaterials 31 (2010) 8097–8105.
[36] M.R. Kano, Y. Bae, C. Iwata, Y. Morishita, M. Yashiro, M. Oka, T. Fujii, A. Komuro, K. Kiyono, M. Kaminishi, K. Hirakawa, Y. Ouchi, N. Nishiyama, K. Kataoka, K. Miyazono, Improvement of cancer-targeting therapy, using nanocarriers for intractable solid tumors by inhibition of TGF-β signaling, Proc. Natl. Acad. Sci. U. S. A. 104 (2007) 3460–3465.